Generalized Hamiltonian for a graphene subjected to arbitrary in-plane strains

Article *in* Functional Materials Letters · February 2015

DOI: 10.1142/S1793604715300017

CITATIONS
2

READS
116

3 authors:

Biao Wang
Sun Yat-Sen University
121 PUBLICATIONS **1,399** CITATIONS
SEE PROFILE

Yunhua Wang
Sun Yat-Sen University
8 PUBLICATIONS **20** CITATIONS
SEE PROFILE

Yulan Liu
Sun Yat-Sen University
207 PUBLICATIONS **3,007** CITATIONS
SEE PROFILE

Feature Article

Functional Materials Letters
Vol. 8, No. 1 (2015) 1530001 (10 pages)

DOI: 10.1142/S1793604715300017

World Scientific
www.worldscientific.com

Generalized Hamiltonian for a graphene subjected to arbitrary in-plane strains

Biao Wang*,‡, Yunhua Wang*,§ and Yulan Liu†,¶
*Sino-French Institute of Nuclear Engineering and Technology
State Key Laboratory of Optoelectronic Materials and Technologies
†School of Engineering, Sun Yat-sen University
510275 Guangzhou, P. R. China
‡wangbiao@mail.sysu.edu.cn
§wangyh22@mail2.sysu.edu.cn
¶stslyl@mail.sysu.edu.cn

Received 31 January 2015; Accepted 3 February 2015; Published 27 February 2015

The interplay between the linear elastic deformation up to 20% and the unique electronic properties of graphene nanostructures offers an attractive prospect to manipulate their properties by strain. Here we review the recent progress on the electronic response of graphene to the in-plane strains, including the strain-modulated electronic structure and the strain-modulated spin, valley and superconducting transports. A generalized Hamiltonian for a graphene was constructed subjected to arbitrary in-plane strains. The Hamiltonian is helpful to design and optimize the graphene-based nano-electromechanical systems (NEMS).

Keywords: Graphene; strain; transport; electronic structure.

1. Introduction

The outstanding mechanical properties of graphene with the Young's modulus of 1 terapascals and the linear elastic deformation more than 20%,[1,2] accompanying the unique electronic structure with the carrier's behavior like relativistic Dirac fermions,[3–5] provide an exciting prospect to design and fabricate the graphene-based nano-electromechanical systems (NEMS).[6–10] Recently, a great deal of theoretical and experimental investigations have been done focusing on the strain effect on the electronic structure, optical properties, electronic transport, spin transport and valley transport in graphene nanostructures and devices. Here we review the recent progresses on the response of graphene to the in-plane strains and construct a generalized Hamiltonian describing the quasiparticles in a graphene subjected to arbitrary in-plane strain. The generalized Hamiltonian is built based on the tight-binding approach and the linear elasticity theory. The tight-binding method for graphene predicts the linear dispersion and zero bandgap,[11] which agrees well with the experimental results.[3–5] The linear elasticity theory for graphene is a reasonable approximation for relative small deformation, since the mechanical experiments demonstrate that the graphene can sustain the linear elastic deformation more than 20%.[1] The tight-binding interaction between any two nearest-neighbor C atoms mainly results from the π bond of the two P_z orbitals, since the in-plane stretch does not lead to the out-of-plane deformation such that the σ bond of the two P_z orbitals is quite weak and can be neglected.[12,13] The generalized Hamiltonian cannot only give the coincident expression as derived before under uniaxial strain, but also be suitable for the tension-shear combined loadings. The analytical expression of the strain-dependent Hamiltonian can be used to predict the electronic properties of the in-plane strained graphene, which is helpful to design and optimize the graphene-based NEMS devices.

2. Model of an in-plane strained graphene

One of the simplest graphene-based NEMS structures is a two-terminal device, as depicted in Fig. 1, where the local strain is usually applied inside the middle region. In order to explore the electronic transport properties along different directions in such a clean and flat graphene nanostructure, one direction should be chosen as the x-axis and then we label the laboratory frame (Cartesian or cylindrical coordinates). It is convenient to choose the longitudinal direction of the device as the x-axis, as shown in the inset in Fig. 1. Note that the longitudinal x direction can be any direction in the graphene plane. That is to say, it is not necessary to require that the zigzag direction of graphene must agree well with the longitudinal x direction. For a two-dimensional material such as the graphene, the in-plane strain tensor in lab frame always

¶Corresponding author.

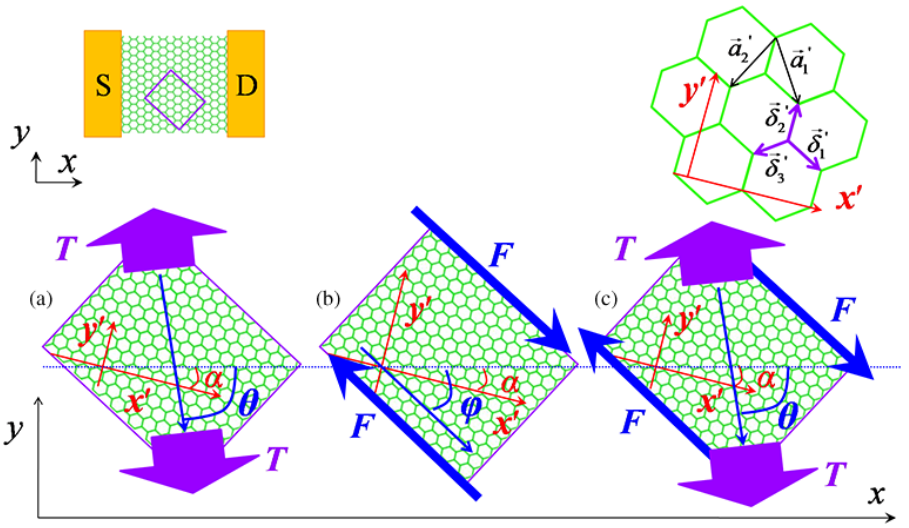

Fig. 1. A two-terminal graphene-based NEMS device (left inset) in the lab frame (x–y frame). The in-plane mechanical loading in the rectangular region possibly includes (a) a uniaxial tension $\boldsymbol{T}$ with the loading directional angle θ, (b) a shear force $\boldsymbol{F}$ with the loading directional angle φ and (c) a tension-shear combined loading. Right inset: Graphene lattice in lattice frame (x'–y' frame).

includes three independent elements ε_{xx}, ε_{yy} and ε_{xy}, no matter which kind of loading is applied in the plane, such as the uniaxial or multiaxial tensions. The strain tensor has this general form

$$\hat{\varepsilon} = \begin{bmatrix} \varepsilon_{xx} & \varepsilon_{xy} \\ \varepsilon_{xy} & \varepsilon_{yy} \end{bmatrix}, \tag{1}$$

where the two elements ε_{xx} and ε_{yy} are the axial strains and ε_{xy} is the shear strain, respectively. Equation (1) indicates that only x and y axial strains retain if ε_{xy} is zero and only pure shear strain exists when both of ε_{xx} and ε_{yy} are zero. Otherwise, the strain tensor reflects a combination of the shearing and axial strains. Provided that a uniaxial tension $\boldsymbol{T}$ is applied along the direction with an angle θ in Fig. 1(a) and the shear force $\boldsymbol{F}$ is applied along the direction with an angle φ in Fig. 1(b), the uniaxial and shear loadings induce the following strain tensors, respectively:

(i) Uniaxial tension induced strain

$$\hat{\varepsilon} = \varepsilon \begin{bmatrix} \cos^2\theta - \upsilon \sin^2\theta & (1+\upsilon)\sin\theta\cos\theta \\ (1+\upsilon)\sin\theta\cos\theta & \sin^2\theta - \upsilon\cos^2\theta \end{bmatrix}, \tag{2a}$$

where ε is the uniaxial strain magnitude and υ is the Poisson's ratio. Note that here the strain tensor always keeps this form, no matter whether the x-axis is the zigzag direction or not, due to the isotropic mechanical property of buck graphene.[14]

(ii) Pure shear force induced strain

$$\hat{\varepsilon} = \gamma \begin{bmatrix} -\sin 2\varphi & \cos 2\varphi \\ \cos 2\varphi & \sin 2\varphi \end{bmatrix}, \tag{2b}$$

where γ is the shear strain magnitude.

The graphene crystal lattice can be described by the translation primitive vectors $\mathbf{a}_1$ and $\mathbf{a}_2$, and the nearest-neighbor vectors $\boldsymbol{\delta}_1$, $\boldsymbol{\delta}_2$ and $\boldsymbol{\delta}_3$ in the lab frame directly, but these vectors have complicated expressions. In order to simplify the expressions of these vectors, we choose another lattice frame (x'–y' frame), where the zigzag direction of graphene has an angle α with respect to the x-axis. In the lattice frame, as depicted in the right inset of Fig. 1, we can simply write these lattice vectors and corresponding basic vectors of reciprocal lattice for the graphene without strain as

$$\begin{aligned} \boldsymbol{\delta}'_1 &= a_0\left(\frac{\sqrt{3}}{2}, -\frac{1}{2}\right), \quad \boldsymbol{\delta}'_2 = a_0(0,1), \\ \boldsymbol{\delta}'_3 &= a_0\left(-\frac{\sqrt{3}}{2}, -\frac{1}{2}\right), \end{aligned} \tag{3a}$$

$$\begin{aligned} \mathbf{a}'_1 &= \boldsymbol{\delta}'_1 - \boldsymbol{\delta}'_2 = a_0\left(\frac{\sqrt{3}}{2}, -\frac{3}{2}\right), \\ -\vec{\mathbf{a}}'_2 &= \vec{\boldsymbol{\delta}}'_3 - \vec{\boldsymbol{\delta}}'_2 = a_0\left(\frac{\sqrt{3}}{2}, \frac{3}{2}\right), \end{aligned} \tag{3b}$$

$$\mathbf{b}'_1 = \frac{2\pi}{a_0}\left(\frac{1}{\sqrt{3}}, -\frac{1}{3}\right), \quad \mathbf{b}'_2 = \frac{2\pi}{a_0}\left(\frac{1}{\sqrt{3}}, \frac{1}{3}\right). \tag{3c}$$

By using the rotation operation $\mathbf{R}(\alpha)$, we can further write all these vectors in the lab frame as

$$\boldsymbol{\chi}^T = \mathbf{R}(\alpha)(\boldsymbol{\chi}')^T = \begin{bmatrix} \cos\alpha & -\sin\alpha \\ \sin\alpha & \cos\alpha \end{bmatrix} (\boldsymbol{\chi}')^T, \tag{4}$$

where $(\boldsymbol{\chi}')^T$ (T denotes the transpose) is any one vector in the lattice frame with its counterpart $\boldsymbol{\chi}^T$ in the lab frame. When an external loading is applied, the graphene structure will have a deformation. As a result, all these vectors in the

lab frame will also be changed and can be described by

$$\boldsymbol{\chi}_i^s = \boldsymbol{\chi}_i + \sum_j \varepsilon_{ij}\boldsymbol{\chi}_j, \tag{5}$$

where $\boldsymbol{\chi}_i^s$ $(i,j = x,y)$ is any deformed vector.

3. The tight-binding Hamiltonian for a strained graphene

3.1. *The tight-binding Hamiltonian and energy band structure of graphene subjected to in-plane strains*

Using the standard nearest-neighbor tight-binding approach, we can write the strain-dependent Hamiltonian in momentum space as

$$H = \begin{bmatrix} 0 & h(\mathbf{k}) \\ h^*(\mathbf{k}) & 0 \end{bmatrix} = \begin{bmatrix} 0 & -\sum_{j=1}^{3} t_j e^{i\mathbf{k}\cdot\boldsymbol{\delta}_j^s} \\ -\sum_{j=1}^{3} t_j e^{-i\mathbf{k}\cdot\boldsymbol{\delta}_j^s} & 0 \end{bmatrix}, \tag{6}$$

where $t_j = V_{pp\pi}(|\boldsymbol{\delta}_j^s|) = -t_0 \exp(-2k_0(|\boldsymbol{\delta}_j^s|/a_0 - 1))$ is the nearest-neighbor hopping integral interactions between the two neighboring carbon P_z orbitals with $k_0 \sim 1.6$.[14] It should be mentioned that the nearest-neighbor hopping integral can also be approximately treated as $t_j = V_{pp\pi}(|\boldsymbol{\delta}_j^s|) = -t_0 a_0^2/|\boldsymbol{\delta}_j^s|^2$, which has been used to evaluate the band energy structure in a graphene ribbon.[15,16] Within the linear deformation range of graphene, the two kinds of approximations have the similar and comparable varying trends. Equation (5) can give the energy band structure (or the dispersion relationship), i.e., $E(\mathbf{k}) = \pm\sqrt{h^*(\mathbf{k})h(\mathbf{k})}$.

From the plot of the energy dispersion relationship, we cannot only observe the strain-induced reciprocal space distortion but also judge whether the bandgap is opened or not. The contour plots of the energy dispersion for strained graphene are shown in Fig. 2. From Fig. 2(a), it can be seen that the Brillouin zone is the typical honeycomb geometry of the hexagonal lattice for free graphene. Assuming that a uniaxial tension along the zigzag direction ($\theta = \alpha = 0$) is applied, the Brillouin zone is apparently stretched and reflects the relatively low symmetry of the rhombic lattice, as shown in Fig. 2(b). The pure shearing strain ($\varphi = \alpha = 0$) in Fig. 2(c) leads to the lowest symmetry of the monoclinic lattice. The strain-induced transformation of the lattice symmetry is given in Ref. 17 and is used to check the electron behavior.[18] Therefore, the strain-induced lattice distortion and the changed hopping interactions of the two P_z orbitals of the neighboring carbon atoms are directly responsible for the electronic structure and transport properties of strained graphene. To make sure that the band gap is opened or not in strained graphene, we plot the band energy structure under different loadings in Fig. 3. It is found that the uniaxial tension cannot open the bandgap even though the strain magnitude is up to 22%, which agrees well with previously theoretical and experimental results.[14,19–21] The pure shear strain less than about 17% cannot either open the bandgap, as shown in Fig. 3(a), where the γ is 15% and φ is zero. But the bandgap can be opened when γ is larger than 17% and also agree well with previous results,[17] as demonstrated in Fig. 3(b), where γ is 20% and φ is zero. In addition, the different combinations of the uniaxial and shear strains have different effects on the bandgap, as shown in Figs. 3(c) and 3(d). The pure shear strains with $\gamma = 15\%$ and $\varphi = 0$, combined with the zigzag direction uniaxial strain with $\varepsilon = 15\%$ and $\theta = 0$ still do not open the gap, but the armchair direction uniaxial strain with $\varepsilon = 15\%$ and $\theta = \pi/2$, combined with the pure shear strain with $\gamma = 15\%$ and $\varphi = 0$ open a wider gap. This means that the uniaxial strains along the zigzag and armchair direction reduces and enhances the pure shear strains with $\varphi = 0$, respectively. Therefore, when using the tension-shear combined loadings one should enhance the shear deformation to realize the off state of a graphene-based NEMS device.

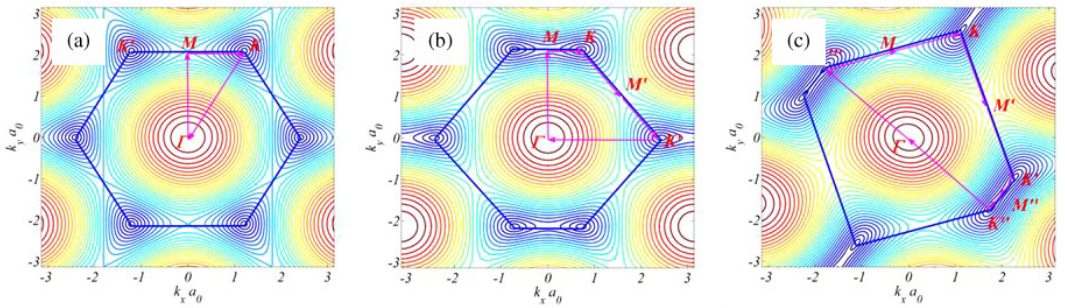

Fig. 2. The contour plots of the energy dispersion for (a) free graphene, (b) graphene under the zigzag direction strain with $\varepsilon = 15\%$ and (c) graphene under pure shear along the zigzag direction with $\gamma = 15\%$. Their irreducible Brillouin zones are defined by Γ—M—K—Γ, Γ—M—K—M—K—Γ and Γ—K—M—K—M—K—M—K—Γ, respectively.

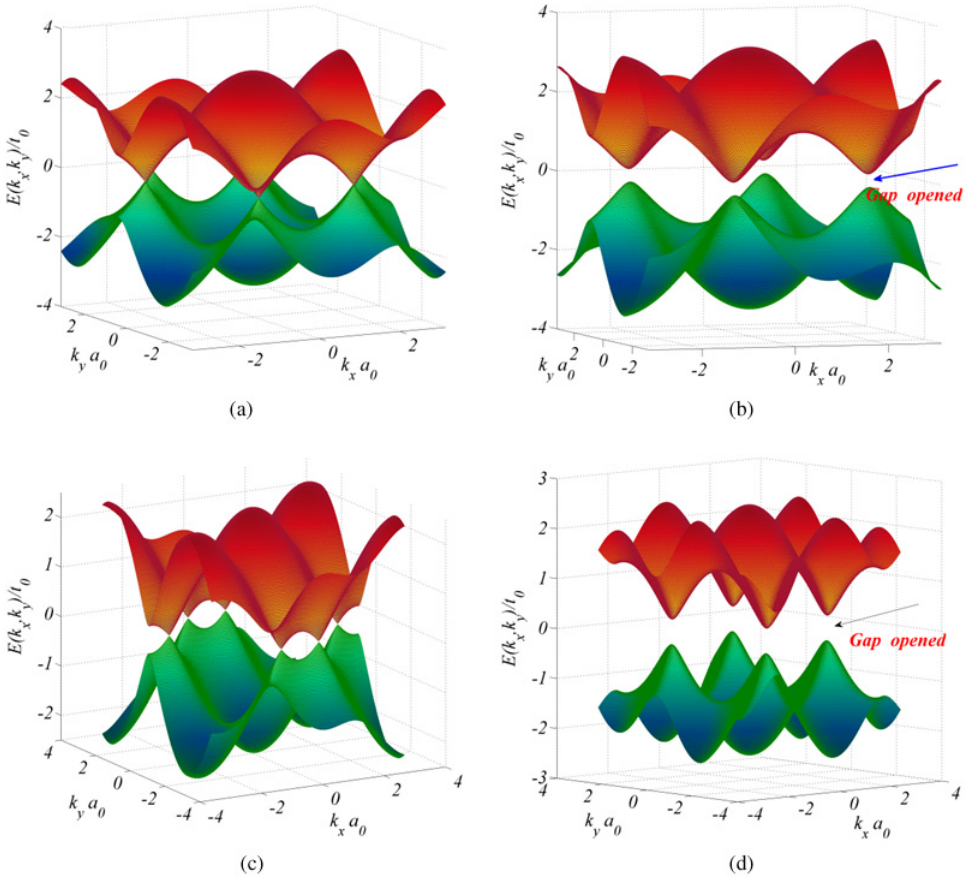

Fig. 3. The energy band structure, under the pure shear strains with $\varphi = 0$ for (a) $\gamma = 15\%$ and (b) $\gamma = 20\%$, under the tension-shear combined loadings for (c) $\gamma = 15\%$, $\varphi = 0$, $\varepsilon = 15\%$ and $\theta = 0$ and (d) $\gamma = 15\%$, $\varphi = 0$, $\varepsilon = 15\%$ and $\theta = \pi/2$.

3.2. *The generalized Hamiltonian within the linear elasticity theory*

By using Eqs. (3)–(6), we can write the term $h(\mathbf{k})$ as

$$\begin{aligned} h(\mathbf{k}) = {} & t_0 f_1 \exp\left[i(k_y \cos\alpha - k_x \sin\alpha)a_0\right] \\ & + \frac{1}{2} t_0 f_2 \exp\left[-\frac{1}{2} i((\sqrt{3}k_x + k_y)a_0 \cos\alpha \right. \\ & \left. + (-k_x + \sqrt{3}k_y)a_0 \sin\alpha)\right] \\ & + \frac{1}{2} t_0 f_3 \exp\left[\frac{1}{2} i((\sqrt{3}k_x - k_y)a_0 \cos\alpha \right. \\ & \left. + (k_x + \sqrt{3}k_y)a_0 \sin\alpha)\right], \end{aligned} \tag{7}$$

where we have set these quantities f_1, f_2 and f_3 as

$$\begin{aligned} f_1 = {} & 1 + i(k_x a_0 \varepsilon_{xy} + k_y a_0 \varepsilon_{yy} + 2ik_0 \varepsilon_{yy} \cos\alpha)\cos\alpha \\ & - i(k_x a_0 \varepsilon_{xx} + k_y a_0 \varepsilon_{xy} + 4ik_0 \varepsilon_{xy} \cos\alpha)\sin\alpha \\ & - 2k_0 \varepsilon_{xx} \sin^2\alpha, \end{aligned} \tag{8a}$$

$$\begin{aligned} f_2 = {} & 2 - 2k_0\varepsilon_{xx} - 2k_0\varepsilon_{yy} - i(\sqrt{3}k_x\varepsilon_{xx} + k_x\varepsilon_{xy} \\ & + \sqrt{3}k_y\varepsilon_{xy} + k_y\varepsilon_{yy})a_0 \cos\alpha \\ & + k_0(-\varepsilon_{xx} - 2\sqrt{3}\varepsilon_{xy} + \varepsilon_{yy})\cos 2\alpha \\ & + i(k_x\varepsilon_{xx} - \sqrt{3}k_x\varepsilon_{xy} + k_y\varepsilon_{xy} - \sqrt{3}k_y\varepsilon_{yy})a_0 \sin\alpha \\ & + k_0(\sqrt{3}\varepsilon_{xx} - 2\varepsilon_{xy} - \sqrt{3}\varepsilon_{yy})\sin 2\alpha, \end{aligned} \tag{8b}$$

$$\begin{aligned} f_3 = {} & 2 - 2k_0\varepsilon_{xx} - 2k_0\varepsilon_{yy} + i(\sqrt{3}k_x\varepsilon_{xx} - k_x\varepsilon_{xy} \\ & + \sqrt{3}k_y\varepsilon_{xy} - k_y\varepsilon_{yy})a_0 \cos\alpha \\ & + k_0(-\varepsilon_{xx} + 2\sqrt{3}\varepsilon_{xy} + \varepsilon_{yy})\cos 2\alpha \\ & + i(k_x\varepsilon_{xx} + \sqrt{3}k_x\varepsilon_{xy} + k_y\varepsilon_{xy} + \sqrt{3}k_y\varepsilon_{yy})a_0 \sin\alpha \\ & + k_0(-\sqrt{3}\varepsilon_{xx} - 2\varepsilon_{xy} + \sqrt{3}\varepsilon_{yy})\sin 2\alpha. \end{aligned} \tag{8c}$$

Note that all these physical quantities are expanded to the first-order of the strain tensor elements and to the second-order in an impulse,[22] due to the assumption of the linear elasticity theory. Using Eqs. (7) and (8a)–(8c), we can find the position (K_{Dx}, K_{Dy}) of the conduction band bottom according to the minimum conditions of the energy function $E(\mathbf{k}) = \sqrt{h^*(\mathbf{k})h(\mathbf{k})}$ in momentum space, and the position of

the conduction band bottom is at

$$K_{Dx}a_0 = \frac{4\pi\cos\alpha}{3\sqrt{3}} - \frac{4\sqrt{3}\pi}{9}(\varepsilon_{xx}\cos\alpha + \varepsilon_{xy}\sin\alpha) + k_0((\varepsilon_{xx}-\varepsilon_{yy})\cos 3\alpha + 2\varepsilon_{xy}\sin 3\alpha), \tag{9a}$$

$$K_{Dy}a_0 = \frac{4\pi\sin\alpha}{3\sqrt{3}} - 2k_0\varepsilon_{xy}\cos 3\alpha - \frac{4\pi}{3\sqrt{3}}(\varepsilon_{xy}\cos\alpha + \varepsilon_{yy}\sin\alpha) + k_0(\varepsilon_{xx}-\varepsilon_{yy})\sin 3\alpha. \tag{9b}$$

By substituting $(k_x, k_y) = (K_{Dx} + q_x, K_{Dy} + q_y)$ into in Eqs. (6) and (7) we can expand the Hamiltonian near the point (K_{Dx}, K_{Dy}) and further evaluate the generalized Hamiltonian as follows:

$$H_S = \begin{bmatrix} 0 & g_1 q_x - i g_2 q_y \\ g_1^* q_x + i g_2^* q_y & 0 \end{bmatrix} = \begin{bmatrix} 0 & \Im_x - i\Im_y \\ \Im_x + i\Im_y & 0 \end{bmatrix} = \boldsymbol{\sigma}\cdot\mathfrak{S} = \boldsymbol{\sigma}\cdot\mathbf{A}\begin{pmatrix} q_x \\ q_y \end{pmatrix}, \tag{10}$$

where $\boldsymbol{\sigma}$ is the Pauli matrice, and the $\hbar v_F = 3t_0/2a_0$ has been set as 1, and the other quantities g_1, g_2, $\Im_x$ and $\Im_y$ with $\lambda = 1/2 - k_0$ are set as

$$g_1 = e^{i\alpha}(1 + 2\lambda(\varepsilon_{xx} - i\varepsilon_{xy})), \tag{11a}$$

$$g_2 = e^{i\alpha}(1 + 2\lambda(\varepsilon_{yy} + i\varepsilon_{xy})), \tag{11b}$$

$$\begin{pmatrix} \Im_x \\ \Im_y \end{pmatrix} = \mathbf{A}\begin{pmatrix} q_x \\ q_y \end{pmatrix} = \begin{bmatrix} (g_1^* + g_1)/2 & i(g_2^* - g_2)/2 \\ (g_1^* - g_1)/2i & (g_2^* + g_2)/2 \end{bmatrix}\begin{pmatrix} q_x \\ q_y \end{pmatrix}, \tag{12a}$$

$$A_{11} = (g_1^* + g_1)/2 = (1 + 2\lambda\varepsilon_{xx})\cos\alpha + 2\lambda\varepsilon_{xy}\sin\alpha, \tag{12b}$$

$$A_{12} = i(g_2^* - g_2)/2 = 2\lambda\varepsilon_{xy}\cos\alpha + (1 + 2\lambda\varepsilon_{yy})\sin\alpha, \tag{12c}$$

$$A_{21} = (g_1^* - g_1)/2i = 2\lambda\varepsilon_{xy}\cos\alpha - (1 + 2\lambda\varepsilon_{xx})\sin\alpha, \tag{12d}$$

$$A_{22} = (g_2^* + g_2)/2 = (1 + 2\lambda\varepsilon_{yy})\cos\alpha - 2\lambda\varepsilon_{xy}\sin\alpha, \tag{12e}$$

Substitutioning of all the matrix elements in Eqs. (12b)–(12e) into Eq. (10) yields the generalized Hamiltonian as

$$H_S = \boldsymbol{\sigma}\cdot\mathfrak{S} = \boldsymbol{\sigma}\cdot\mathbf{R}(-\alpha)(\hat{\mathbf{I}} + 2\lambda\hat{\varepsilon})\mathbf{q}, \tag{13}$$

where $\boldsymbol{R}(-\alpha)$ is the rotation operation as demonstrated in Eq. (4) and $\hat{\mathbf{I}}$ is the identity matrix.

The validity of the generalized Hamiltonian in Eq. (13) is checked by comparison with previous results. We first check the special uniaxial tension, as done in Refs. 14 and 22, where the angle θ of the tension direction is fixed along the x-axis (i.e., $\theta = 0$), but the angle α can be varied to determine which direction of the graphene lattice is stretched. By substituting the strain tensor in Eq. (2a) into Eq. (13), we can obtain the Hamiltonian under uniaxial strain as follows:

$$H_S = \boldsymbol{\sigma}\cdot\mathfrak{S} = \boldsymbol{\sigma}\cdot\mathbf{A}\begin{pmatrix} q_x \\ q_y \end{pmatrix} = \boldsymbol{\sigma}\cdot\begin{bmatrix} \cos\alpha & \sin\alpha \\ -\sin\alpha & \cos\alpha \end{bmatrix}\begin{pmatrix} (1+2\lambda\varepsilon)q_x \\ (1-2\lambda\varepsilon\upsilon)q_y \end{pmatrix}. \tag{14}$$

The obtained Hamiltonian for the uniaxial tension is consistent with the results in Refs. 22.When the strain magnitude ε is lower than 20%, the band gap is not opened. As a result, the conduction band bottom is the so-called Dirac point. The Hamiltonian in Eq. (14) near the Dirac point directly demonstrates the anisotropic linear energy dispersion

$$E^2(\mathbf{k}) = (1 + 2\lambda\varepsilon)^2 q_x^2 + (1 - 2\lambda\varepsilon\upsilon)^2 q_x^2. \tag{15}$$

For example, the effects of the zigzag direction strain on the linear energy dispersion are shown in Figs. 4(a) and 4(b) with $\varepsilon = 5\%$ and 15%, respectively. Due to the isotropic dispersion, the isoenergetic curves for free graphene are circles. In the presence of the zigzag direction strain, the isoenergetic curves are ellipses, which reflect the typical anisotropic dispersion. In addition, with the increased strain, the anisotropy is enhanced. Similarly, we find the shear strain can also induce anisotropic linear energy dispersion, but with a rotation due to the shear force, as shown in Fig. 4(c) with $\gamma = 15\%$, $\varphi = 0$.

Substituting the strain tensor in Eq. (2a) into Eqs. (9a)–(9b), respectively, we can write the position of Dirac point for

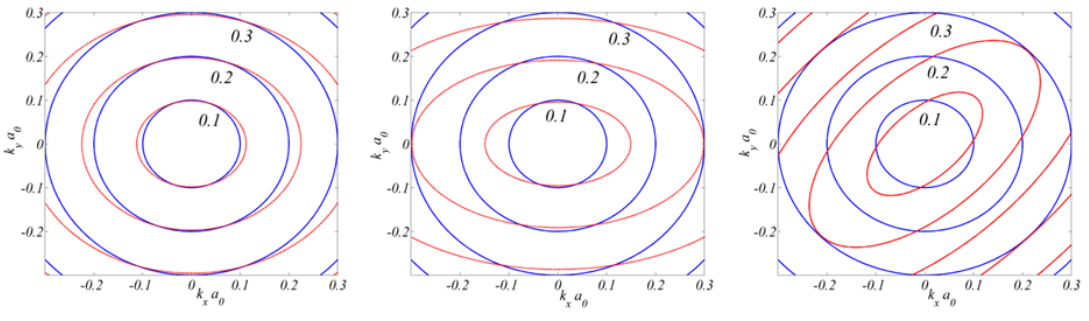

Fig. 4. Strain-induced anisotropic isoenergetic curves under zigzag direction strain for (a) $\varepsilon = 5\%$ and (b) $\varepsilon = 15\%$, under the pure shear strain for (c) $\gamma = 15\%$, $\varphi = 0$. The circles are the isoenergetic curves of free graphene.

the uniaxial tension, as follows:

$$K_{Dx}a_0 = \frac{4\sqrt{3}\pi}{9}(1-\varepsilon)\cos\alpha + k_0\varepsilon(1+\upsilon)\cos 3\alpha, \quad (15a)$$

$$K_{Dy}a_0 = \frac{4\sqrt{3}\pi}{9}(1+\varepsilon\upsilon)\sin\alpha + k_0\varepsilon(1+\upsilon)\sin 3\alpha. \quad (15b)$$

The position of Dirac point in Eqs. (15a) and (15b) includes the shift of the Dirac point, i.e., the strain-dependent components, which play the role on the strain-induced pseudomagnetic field,[8–10,23–27] and can be experimentally[7,28–31] probed. This is very important for electronic transport in graphene nanostructure. Note that if a uniform strain is applied inside the whole graphene layer, there is no pseudomagnetic field, since the mismatch of the wave vector never happens.

In principle, the generalized Hamiltonian in Eq. (13) can be used to deal with any in-plane strains, in spite of the non-uniform strain profiles, strain gradient and boundary problems. The reason is that one can use the finite difference method or finite element method to separate the strained regions into a series of small and uniform strained modules, where a reasonable size $a \times b$ of the small and uniform two-dimensional module must be much bigger than the lattice constant a_0 (i.e., $a, b \gg a_0$) to ensure the validity of the generalized Hamiltonian. In addition, it is worthy to mention that the finite difference method has been successfully applied to predict the electronic properties of graphene quantum waveguide and superlattice,[22,32–40] and the predicted results agree well with the experiment, which indicates that the Dirac point can be cloned in a graphene superlattice.[41] The limitations of the generalized Hamiltonian in Eq. (13) are only for in-plane strain under the small deformation, where the maximum limit of the uniaxial strain is about 20% and the maximum shear strain is about 15%, since a larger shear strain can open the band gap and possibly destroy the graphene crystal lattice.

Experimentally, the in-plane strain can be realized by the flexible substrate (such as the polyethylene terephthalate),[1,2,42] where a robust adhesion between the graphene and the substrate is made to ensure the effective uniaxial loading on the graphene. Usually, for a two-terminal graphene-based NEMS device, the uniform external tension is applied along the longitudinal transport direction in lab frame. In such a case, the angle θ equals to zero, and therefore the longitudinal tension along the x-axis is relatively easy to be loaded in experiments[42] and becomes simple for the theoretical analysis.

4. Strain effects on the quantum transport in graphene nanostructure

4.1. *Strain-manipulated electronic transports in graphene nanostructure*

Owing to the linear dispersion and the ultra-long mean free path with the order of micrometer, the electrons and holes as relativistic Dirac fermions show the ballistic electronic transport phenomenon in clean graphene.[3–5] How to control the electronic transport behavior in graphene has aroused a great deal of attention of many researchers. The electrons in graphene can perfectly pass through a potential barrier with normal incidence and this phenomenon is the so-called Klein tunneling.[43,44] In the presence of a bipolar PN junction fabricated by a combination of top/bottom electrostatic gates,[46–48] the carriers exhibit electronic negative refractive due to the interband scattering,[49] which attracts considerable attention on the analogous light phenomenon of electrons in graphene-based nanostructure.[50–59] Alternatively, the strain opens an exotic way to tailor the electronic transport in a strain-engineering fashion, where the electronic confinement, collimation and scattering can be achieved by designing an expected substrate-induced local strain profile.[8] For the strain-induced graphene 1D channels, i.e., the quantum waveguide, the bound states and the surface modes occur and play the important role of guided mode on guiding the electrons inside the channel.[8,58,59] In addition, the different directional strains lead to different effects on the guided mode and the strain-tunable bound states are verified by the photon-assisted tunneling,[59] where an oscillating potential or a laser is used to supply the photon.[60–71] A profile of periodic local uniaxial strains or corrugated deformation in graphene can remarkably affect the energy structure, electronic transmission and shot noise by the strain-induced vector potential, scalar potential and renormalized group velocity.[22,37–40] In addition, the anisotropic energy dispersion in graphene potential superlattice also exists in the graphene strain superlattice.[35] Attractively, a zero-field quantum Hall effect can appear in strained graphene,[9] due to the strain-induced pseudomagnetic field up 10–100 T, which has been confirmed by experiments.[7] The strain also has remarkable tunable effects on the optical properties of graphene, because the strain changes the lattice space group and the energy structure.[72–74]

4.2. *Strain-manipulated graphene Spin electronics and Valley electronics*

Experiments demonstrate that the spin coherence length in graphene at room temperature can be more than 1 μm.[75] The combination of the ultra-long spin coherence and the unique electronic structure of graphene have attracted considerable attention in graphene-based spintronics and quantum transports in low-dimensional nanostructure. Because two degenerate and inequivalent valleys at the K and K' corner of the Brillouin zone exist in graphene, the valley degree of freedom plays the role as the similar spin information carrier. When the valley freedom can be manipulated in a controllable fashion, as a counterpart of the spintronics, the

graphene-based valleytronics can spring up attractively.[76] For the graphene spintronics, to inject and detect the spin in graphene, a spin valve can be fabricated with an enhanced injecting efficiency.[77–81] The reduced size and edge effects may make magnetic correlations happen in a graphene nanoflake[82,83] and a zigzag graphene ribbon subjected to an in-plane electric field may have complete single spin state.[84,85] Alternatively, the extrinsic Rashba spin–orbit interaction (SOI) in graphene can induce the spin-dependent electronic structure,[86–93] and has been demonstrated in experiments, where the graphene is grown on a metal Ni substrate.[94,95] Recently, Rashba SOI is extensively used in the tunable spin transport.[96–104] Another way is the proximity effect between a ferromagnetic insulator and graphene,[105] which induces the ferromagnetic graphene and has been demonstrated in experiments.[106,107] For the graphene valleytronics, the valley valve, filter and polarization also need to be realized. A zigzag graphene ribbon with size confinement and additional gate voltage can provide the valley filter and valve effects.[76] The different non-trivial deformations (i.e., band trigonal warping effect) for the energy band of the two valleys will happen if a relatively high voltage ($\sim$600 meV) is applied, and provide another way to realize the valley polarization.[108,109] In addition, the intense irradiation on graphene or inducing Dirac gap can also induce the valley polarization effect.[110]

Besides the generation of the spin polarization and the valley polarization, the controllable spin and valley transports in graphene need to be realized. In such a case, strains provide an important way to manipulate the spin and valley transports in graphene-based nanostructure. There are two ways for strain in graphene to modulate the spin and valley transports. One is that designing an expected substrate pattern induces a suitable strain distribution, which produces pseudomagnetic vector potential to have remarkable effects on the electronic transports; and the other one is that using the uniaxial tension to induce not only the anisotropic strain-renormalized group velocity but also the pseudomagnetic field from the shift of the Dirac point to manipulate the spin and valley electrons in graphene nanostructure. First, for the spin manipulation, a ferromagnetic/strained/normal graphene junction demonstrates a strain-controllable spin-resolved Fermi energy range and a strain-modulated spin rectification, which can be utilized as a tunable spin diode.[111] It is shown that the zigzag and armchair direction strains have anisotropic modulating effects. A graphene ferromagnetic junction coupled with the pseudomagnetic vector potential shows a strain-tunable spin-resolved conductance and polarization, which can be used as a spin filter.[112] The strain combining with a spin–orbit coupling can also have a tunable effect on the spin-dependent conductance modulation[113] and the generation of full spin polarization if a ferromagnetic exchange splitting is induced.[114] The strain effects on the spin transport exhibit a different tunable behavior from the gate-controlled potential barrier.[115] Next, for the valley manipulation, a combination of the strain and real magnetic field in graphene can realize the valley polarization, since the symmetry of strain-induced vector potential at valleys K and K′ is destroyed by the real magnetic field.[116–119] Consequently, the combined structures between the local strain and real magnetic field can be designed to tune the valley transport in graphene.[120–124]

4.3. *Strain-manipulated graphene superconductor nanoelectronics*

Experiments demonstrate that the superconductivity of graphene cannot only be induced by the proximity effects,[125–134] but also be applied in a graphene-superconductor junction, where the relativistic DC Josephson current is observed and agree well with the theoretical results.[135–141] The interplay between the superconductivity and the linear dispersion of graphene is responsible for not only the specular Andreev reflection,[142–149] but also the unusual supercurrent phenomenon (i.e., a finite Josephson current induced by the zero energy state), while controllable superconductor nanoelectronics require a high on/off rate. Therefore, controllable Josephson current in graphene superconductor junction needs to be realized.

The strain in graphene can not only induce the size deformation but also supply an anisotropic manipulation on the supercurrent due to the anisotropic group velocity and the different Dirac point displacements. In addition, the strain has little influence on the superconducting state of graphene under the superconducting electrodes, because the strain-induced pseudomagnetic fields have no impacts on the spin unlike the real magnetic field.[150] There are two ways to realize the strain-modulated graphene Josephson junction. One is the uniform strain for the whole graphene superconductor junction including the left and right graphene superconducting regions,[151–153] and the other is the non-uniform strain only applied inside some local regions.[154]

For the uniform strain, the whole sheet of graphene has the same deformation and thus there is no mismatch of the wave vectors of the wave functions between the superconducting region and the normal region. In such a case, the strain-induced size deformation plays the most important role in tuning the Josephson current at the charge neutrality point.[151] The critical supercurrent I_C at the Dirac point is proportional to the rate between the width W and the length L of the middle normal region in the graphene Josephson junction, (i.e., $I_C \sim W/L$).[135] As a result, the zigzag and armchair direction strains lead to the opposite effects on the supercurrent, i.e., linearly decreasing and increasing, respectively. The clear

reason is that the horizontal and vertical tensions induce the opposite size deformation of W/L. But note that under armchair direction strain, the supercurrent direction is perpendicular to the strain direction, which is different from the work in Ref. 154, where the electronic transport direction always keeps the same direction as the strain direction. The critical supercurrent I_C at other energy has a similar changing trend, but will oscillate when a potential barrier is applied in the middle region.[139] In addition, a ferromagnetic grapheme coupled with strain in the middle region, 0–π state transition of supercurrent will happen and the 0–π state transition can be manipulated by the zigzag direction strain.[155] The uniform strain can also be applied to change the tunneling conductance in a graphene-based normal/insulator/superconductor junction[153] and tune the superconducting pair correlation and display the interplay between the strain-induced pseudomagnetic fields and pair correlations.[150] When a local strain is applied inside the middle region of a Josephson junction, some obviously different effects of the local strain on the supercurrent can be predicted. Firstly, a velocity distribution occurs due to the unequal group velocities in different regions. The velocity distribution will have obvious influence on electronic transport,[156] and thus change the oscillating period of supercurrent when the zigzag direction strain is applied, but note that in such a case the zigzag direction strain never induced the mismatch of the wave vector k_y due to $K_{Dy} = 0$. Second, when the armchair direction strain is applied, the mismatch of the wave vectors k_y exists due to the Dirac point displacement, which leads to the vanishing of the Andreev bound states and turns off the Josephson supercurrent with a cutoff strain. But one should bear in mind that here the supercurrent direction is the same as the strain direction.

In summary, the effects of the in-plane strain on the electronic structure and the spin, valley and superconducting transports are summarized and reviewed. A generalized Hamiltonian in graphene subjected to arbitrary in-plane strains is constructed. By comparing with previous results, it is found that the generalized Hamiltonian is effective and has more general characteristics for graphene under in-plane complex strain state.

Acknowledgments

We are grateful for the support from the National Natural Science Foundation through the funds (Nos. 11232015, 10572155, 11472313), and the Research Fund for the Doctoral Program of Higher Education of China (Nos. 20120171110005, 20130171130003).

References

1. C. Lee *et al.*, *Science* **321**, 385 (2008).
2. K. S. Kim *et al.*, *Nature* **457**, 706 (2009).
3. K. S. Novoselov *et al.*, *Science* **306**, 666 (2004).
4. K. S. Novoselov *et al.*, *Nature* **438**, 197 (2005).
5. Y. Zhang *et al.*, *Nature* **438**, 201 (2005).
6. J. S. Bunch *et al.*, *Science* **315**, 490 (2007).
7. N. Levy *et al.*, *Science* **329**, 544 (2010).
8. V. M. Pereira and A. H. Castro Neto, *Phys. Rev. Lett.* **103**, 046801 (2009).
9. F. Guinea, M. I. Katsnelson and A. K. Geim, *Nat. Phys.* **6**, 30 (2010).
10. F. de Juan *et al.*, *Nat. Phys.* **7**, 810 (2011).
11. A. H. Castro Neto *et al.*, *Rev. Mod. Phys.* **81**, 109 (2009).
12. J. L. Manes *et al.*, *Phys. Rev. B* **88**, 155405 (2013).
13. M. A. H. Vozmediano, M. I. Katsnelson and F. Guinea, *Phys. Rep.* **496**, 109 (2010).
14. V. M. Pereira, A. H. Castro Neto and N. M. R. Peres, *Phys. Rev. B* **80**, 045401 (2009).
15. Y. Li *et al.*, *Nano Res* **3**, 545 (2010).
16. Y. Lu and J. Guo, *Nano Res.* **3**, 189 (2010).
17. G. Cocco, E. Cadelano and L. Colombo, *Phys. Rev. B* **81**, 241412 (R) (2010).
18. M. Oliva-Leyva and Gerardo G. Naumis, *Phys. Rev. B* **88**, 085430 (2013).
19. S. M. Choi, S. H. Jhi and Y. W. Son, *Phys. Rev. B* **81**, 081407 (R) (2010).
20. Z. H. Ni *et al.*, *ACS Nano* **2**, 2301 (2008).
21. M. Y. Huang *et al.*, *Nano Lett.* **10**, 4074 (2010).
22. F. M. D. Pellegrino, G. G. N. Angilella and R. Pucci, *Phys. Rev. B* **84**, 195404 (2011).
23. F. Guinea, M. I. Katsnelson and M. A. H. Vozmediano, *Phys. Rev. B* **77**, 075422 (2008).
24. M. Ramezani Masir, D. Moldovan and F. M. Peeters, *Solid State Commun.* **175**, 76 (2013).
25. M. Neek-Amal and F. M. Peeters, *Phys. Rev. B* **85**, 195445 (2012); *ibid*, **85**, 195446 (2012).
26. A. L. Kitt, Vitor M. Pereira, Anna K. Swan and Bennett B. Goldberg, *Phys. Rev. B* **85**, 115432 (2012); *ibid*, **87**, 159909 (E) (2013).
27. Y. Chang, T. Albash and S. Haas, *Phys. Rev. B* **86**, 125402 (2012).
28. H. Yan *et al.*, *Phys. Rev. B* **85**, 035422 (2012).
29. H. Yan *et al.*, *Phys. Rev. B* **87**, 075405 (2013).
30. W.-Y. He *et al.*, *Phys. Rev. B* **89**, 125418 (2014).
31. M. Yang *et al.*, *J. Appl. Phys.* **112**, 073710 (2012).
32. J. R. Williams *et al.*, *Nature Nano.* **6**, 222 (2011).
33. M. Barbier, P. Vasilopoulos and F. M. Peeters, *Phys. Rev. B* **81**, 075438 (2010).
34. L. G. Wang and S. Y. Zhu, *Phys. Rev. B* **81**, 205444 (2010).
35. C.-H. Park *et al.*, *Nat. Phys.* **4**, 213 (2008).
36. L. Brey and H. A. Fertig, *Phys. Rev. Lett.* **103**, 046809 (2009).
37. A. Isacsson *et al.*, *Phys. Rev. B* **77**, 035423 (2008).
38. F. Guinea and T. Low, *Philos. Trans. R. Soc. London Ser. A* **368**, 5391 (2010).
39. I. I. Naumov and A. M. Bratkovsky, *Phys. Rev. B* **84**, 245444 (2011).
40. S. Gattenlöhner, W. Belzig and M. Titov, *Phys. Rev. B* **82**, 155417 (2010).
41. L. A. Ponomarenko *et al.*, *Nature (London)* **497**, 594 (2013).
42. T. M. G. Mohiuddin *et al.*, *Phys. Rev. B* **79**, 205433 (2009).
43. M. I. Katsnelson, K. S. Novoselov and A. K. Geim, *Nat. Phys.* **2**, 620 (2006).
44. A. F. Young and P. Kim, *Nat. Phys.* **5**, 222 (2009).

45. B. Özyilmaz *et al.*, *Phys. Rev. Lett.* **99**, 166804 (2007).
46. B. Huard *et al.*, *Phys. Rev. Lett.* **98**, 236803 (2007).
47. J. R. Williams, L. DiCarlo and C. M. Marcus, *Science* **317**, 638 (2007).
48. T. Ihn *et al.*, *Mater. Today* **13**, 44 (2010).
49. V. V. Cheianov, V. Fal'ko and B. L. Altshuler, *Science* **315**, 1252 (2007).
50. J. Cserti, A. Pályi and C. Péterfalvi, *Phys. Rev. Lett.* **99**, 246801 (2007).
51. C. W. J. Beenakker *et al.*, *Phys. Rev. Lett.* **102**, 146804 (2009).
52. C. E. P. Villegas and Marcos R. S. Tavares, *Appl. Phys. Lett.* **101**, 163104 (2012).
53. A. V. Rozhkov *et al.*, *Phys. Rep.* **503**, 77 (2011).
54. Y. P. Bliokh, V. Freilikher and F. Nori, *Phys. Rev. B* **81**, 075410 (2010).
55. J. Milton Pereira *et al.*, *Phys. Rev. B* **74**, 045424 (2006).
56. F. Zhang *et al.*, *Appl. Phys. Lett.* **94**, 212105 (2009).
57. Z. Wu, *Appl. Phys. Lett.* **98**, 082117 (2011).
58. F. M. D. Pellegrino, G. G. N. Angilella and R. Pucci, *Phys. Rev. B* **85**, 195409 (2012).
59. Y. Wang, Y. Liu and B. Wang, *Appl. Phys. Express* **6**, 065102 (2013).
60. J.-F. Liu and K. S. Chan, *Nanotechnology* **22**, 395201 (2011).
61. L. E. F. Foa Torres *et al.*, *Appl. Phys. Lett.* **99**, 092102 (2011).
62. W. Lu *et al.*, *J. Appl. Phys.* **111**, 103717 (2012).
63. P. San-Jose *et al.*, *Phys. Rev. B* **84**, 155408 (2011).
64. L. H. Ingaramo and L. E. F. Foa Torres, *Appl. Phys. Lett.* **103**, 123508 (2013).
65. Y. Zhou and M. W. Wu, *Phys. Rev. B* **86**, 085406 (2012).
66. Q. Zhang, K. S. Chan and Z. Lin, *Appl. Phys. Lett.* **98**, 032106 (2011).
67. C. Benjamin, *Appl. Phys. Lett.* **103**, 043120 (2013).
68. N. Myoung, G. Ihm and K. Seo, *Curr. Appl. Phys.* **13**, 1335 (2013).
69. D. Bercioux *et al.*, *Appl. Phys. Lett.* **101**, 122405 (2012).
70. C. Sinha and R. Biswas, *Phys. Rev. B* **84**, 155439 (2011).
71. M. A. Zeb, K. Sabeeh and M. Tahir, *Phys. Rev. B* **77**, 165402 (2008).
72. V. M. Pereira *et al.*, *Europhys. Lett.* **92**, 67001 (2010).
73. F. M. D. Pellegrino, G. G. N. Angilella and R. Pucci, *Phys. Rev. B* **81**, 035411 (2010).
74. F. Qi and G. Jin, *J. Appl. Phys.* **114**, 073509 (2013).
75. N. Tombros *et al.*, *Nature* **448**, 571 (2007).
76. A. Rycerz, J. Tworzydło and C. W. J. Beenakker, *Nat. Phys.* **3**, 172 (2007).
77. W. Han *et al.*, *J. Magn. Magn. Mater.* **324**, 369 (2012).
78. E. W. Hill *et al.*, *IEEE Trans. Magn.* **42**, 2694 (2006).
79. M. Ohishi *et al.*, *Jpn. J. Appl. Phys.* **46**, L605 (2007).
80. C. Józsa *et al.*, *Phys. Rev. Lett.* **100**, 236603 (2008).
81. S. Cho, Y. F. Chen and M. S. Fuhrer, *Appl. Phys. Lett.* **91**, 123105 (2007).
82. O. V. Yazyev, *Rep. Prog. Phys.* **73**, 056501 (2010).
83. W. L. Wang, S. Meng and E. Kaxiras, *Nano Lett.* **8**, 241 (2008).
84. Y.-W. Son, M. Cohen and S. G. Louie, *Nature* **444**, 347 (2006).
85. E.-J. Kan *et al.*, *Appl. Phys. Lett.* **91**, 243116 (2007).
86. C. L. Kane and E. J. Mele, *Phys. Rev. Lett.* **95**, 146802 (2005).
87. H. Min *et al.*, *Phys. Rev. B* **74**, 165310 (2006).
88. E. I. Rashba, *Phys. Rev. B* **79**, 161409 (2009).
89. A. H. Castro Neto and F. Guinea, *Phys. Rev. Lett.* **103**, 026804 (2009).
90. Z. Qiao *et al.*, *Phys. Rev. B* **82**, 161414 (2010).
91. T. Stauber and J. Schliemann, *New J. Phys.* **11**, 115003 (2009).
92. D. H. Hernando, F. Guinea and A. Brataas, *Phys. Rev. Lett.* **103**, 146801 (2009).
93. W.-K. Tse *et al.*, *Phys. Rev. B* **83**, 155447 (2011).
94. A. Varykhalov *et al.*, *Phys. Rev. Lett.* **101**, 157601 (2008).
95. O. Rader *et al.*, *Phys. Rev. Lett.* **102**, 057602 (2009).
96. D. Bercioux and A. De Martino, *Phys. Rev. B* **81**, 165410 (2010).
97. C. Bai *et al.*, *Appl. Phys. Lett.* **96** (2010) 223102.
98. K. Shakouri *et al.*, *Phys. Rev. B* **88**, 115408 (2013).
99. E. Faizabadi and F. Sattari, *J. Appl. Phys.* **111**, 093724 (2012).
100. M. H. Liu, J. Bundesmann and K. Richter, *Phys. Rev. B* **85**, 085406 (2012).
101. Q. Zhang, Z. Lin and K. S. Chan, *Appl. Phys. Lett.* **102**, 142407 (2013).
102. M. M. Asmar and S. E. Ulloa, *Phys. Rev. B* **87**, 075420 (2013).
103. Z. Liu *et al.*, *J. Appl. Phys.* **115**, 203710 (2014).
104. A. Lopez, Z. Z. Sun and J. Schliemann, *Phys. Rev. B* **85**, 205428 (2012).
105. H. Haugen, D. Huertas-Hernando and A. Brataas, *Phys. Rev. B* **77**, 115406 (2008).
106. A. G. Swartz *et al.*, *ACS Nano* **6**, 10063 (2012).
107. J. Klinkhammer *et al.*, *Appl. Phys. Lett.* **103**, 131601 (2013).
108. J. L. Garcia-Pomar, A. Cortijo and M. Nieto-Vesperinas, *Phys. Rev. Lett.* **100**, 236801 (2008).
109. M. Pereira *et al.*, *J. Phys.: Condens. Matter* **21**, 045301 (2009).
110. D. S. L. Abergel and T. Chakraborty, *Appl. Phys. Lett.* **95**, 062107 (2009).
111. Y. Wang, Y. Liu and B. Wang, *Appl. Phys. Lett.* **105**, 052409 (2014).
112. F. Zhai and L. Yang, *Appl. Phys. Lett.* **98**, 062101 (2011).
113. Z. Cao *et al.*, *Appl. Phys. Lett.* **105**, 172407 (2014).
114. Q. Wu *et al.*, *Appl. Phys. Lett.* **105**, 252402 (2014).
115. T. Yokoyama, *Phys. Rev. B* **77**, 073413 (2008).
116. Z. Wu *et al.*, *Phys. Rev. Lett.* **106**, 176802 (2011).
117. F. Zhai *et al.*, *Phys. Rev. B* **82**, 115442 (2010).
118. T. Fujita, M. B. A. Jalil and S. G. Tan, *Appl. Phys. Lett.* **97**, 043508 (2010).
119. T. Low and F. Guinea, *Nano Lett.* **10**, 3551 (2010).
120. Z. Khatibi, H. Rostami and Reza Asgari, *Phys. Rev. B* **88**, 195426 (2013).
121. Z. Niu, *J. Appl. Phys.* **111**, 103712 (2012).
122. Y. Zhang and F. Zhai, *J. Appl. Phys.* **111**, 033705 (2012).
123. J. Wang, K. S. Chan and Z. Lin, *Appl. Phys. Lett.* **104**, 013105 (2014).
124. H. Rostami and Reza Asgari, *Phys. Rev. B* **86**, 155435 (2012).
125. H. B. Heersche *et al.*, *Nature* **446**, 56 (2007).
126. X. Du, I. Skachko and E. Y. Andrei, *Phys. Rev. B* **77**, 184507 (2008).
127. U. C. Coskun *et al.*, *Phys. Rev. Lett.* **108**, 097003 (2012).
128. I. V. Borzenets *et al.*, *Phys. Rev. Lett.* **107**, 137005 (2011).
129. G. H. Lee *et al.*, *Phys. Rev. Lett.* **107**, 146605 (2011).
130. A. Shailos *et al.*, *Europhys. Lett.* **79**, 57008 (2007).
131. J. H. Choi *et al.*, *Nat. Commun.* **4**, 2525 (2013).
132. N. Mizuno, B. Nielsen and X. Du, *Nat. Commun.* **4**, 2716 (2013).

133. T. Dirks *et al.*, *Nat. Phys.* **7**, 386 (2011).
134. Z. Han *et al.*, *Nat. Phys.* **10**, 380 (2014).
135. M. Titov and C. W. J. Beenakker, *Phys. Rev. B* **74**, 041401 (R) (2006).
136. A. G. Moghaddam and M. Zareyan, *Phys. Rev. B* **74**, 241403 (R) (2006).
137. J. González and E. Perfetto, *Phys. Rev. B* **76**, 155404 (2007).
138. I. Hagymási, A. Kormányos and J. Cserti, *Phys. Rev. B* **82**, 134516 (2010).
139. M. Maiti and K. Sengupta, *Phys. Rev. B* **76**, 054513 (2007).
140. A. M. Black-Schaffer and S. Doniach, *Phys. Rev. B* **78**, 024504 (2008).
141. J. Linder *et al.*, *Phys. Rev. Lett.* **100**, 187004 (2008).
142. C. W. J. Beenakker, *Rev. Mod. Phys.* **80**, 1337 (2008).
143. Q. Zhang *et al.*, *Phys. Rev. Lett.* **101**, 047005 (2008).
144. J. Linder, M. Zareyan and A. Sudbo, *Phys. Rev. B* **80**, 014513 (2009).
145. S. Cheng *et al.*, *Phys. Rev. Lett.* **103**, 167003 (2009).
146. C. Bai, Y. Yang and X. Zhang, *Appl. Phys. Lett.* **92**, 102513 (2008).
147. J. Wang and S. Liu, *Phys. Rev. B* **85**, 035402 (2012).
148. Y. S. Ang, Z. Ma and C. Zhang, *Sci. Rep.* **2**, 1013 (2012).
149. X. Zhai and G. Jin, *Phys. Rev. B* **89**, 085430 (2014).
150. L. Covaci and F. M. Peeters, *Phys. Rev. B* **84**, 241401(R) (2011).
151. M. Alidoust and J. Linder, *Phys. Rev. B* **84**, 035407 (2011).
152. B. Soodchomshom, I. M. Tang and R. Hoonsawat, *J. Supercond. Nov. Magn.* **25**, 1787 (2012).
153. M. Khezerlou *et al.*, *Superlattices Microstruct.* **63**, 58 (2013).
154. Y. Wang, Y. Liu and B. Wang, *Appl. Phys. Lett.* **103**, 182603 (2013).
155. J. Zou and G. Jin, *Appl. Phys. Lett.* **98**, 122106 (2011).
156. Y. Wang, Y. Liu and B. Wang, *Physica E* **53**, 186 (2013).